Fuel 296 (2021) 120529

Contents lists available at ScienceDirect

Fuel

journal homepage: www.elsevier.com/locate/fuel

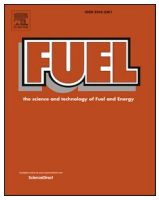

Full Length Article

Development and assessment of a cleaner locomotive powering system with alternative fuels

Shaimaa Seyam, Ibrahim Dincer, Martin Agelin-Chaab

Dept. of Automotive, Mechanical and Manufacturing Engineering, Ontario Tech University, Oshawa, Ontario, Canada

ARTICLE INFO

Keywords:
Gas turbine
Molten carbonate fuel cell
Alternative fuels
Energy
Exergy
Efficiency

ABSTRACT

Transportation research is critical in every domain of the transportation sector, including the rail sector. For sustainable rail transportation, alternative/cleaner powering options are badly needed which can only be possible with cleaner fuels. This paper presents a proposed hybrid combined engine system consisting of a gas turbine and a molten carbonate fuel cell combined with an internal combustion engine. The proposed system uses ecofriendly fuels in order to increase the engine performance and reduce carbon emissions. The hybrid combined engine is modeled using Aspen Plus and is thermodynamically analyzed. The alternative fuels chosen for this study are hydrogen, methanol, ethanol, and dimethyl ether. It was found that the proposed powering system can produce 4200 kW, which is doubled the power of the internal combustion engine, with 43% and 55% thermal and exergetic efficiencies, respectively. The cooling load of the absorption refrigeration system varies from 442 kW to 615 kW with maximum energetic and exergetic co-efficient of performances of 18.29% and 9.54%, respectively. The CO_2 emissions dropped by more than 60% using alternative fuels. In addition, parametric studies are conducted in the operating pressure of the molten carbonate fuel cell (MCFC) and gas turbine (GT). The best performance can be fulfilled at 200 kPa for the MCFC and 900 kPa for the GT. Therefore, the hybrid combined engine can provide high power with less CO_2 emissions and high performance.

1. Introduction

The population of Canada is increasing at a rate of 1% and thus necessitating an increase in different transportation modes to facilitate the mobility of people, goods, and services across the country and the world [1]. Thus, transportation significantly impacts the economic, social, and political state of the country. Natural Resources Canada's report of 2019 [2] stated that the total transportation energy use increased by 16% from 2000 to 2016 to a total of 2,683 PJ in 2016. The contributions of fuels to the total energy use are motor gasoline with 58% and diesel fuel oil of 28%. The fuel consumption has a significant impact on the environment. The greenhouse gas (GHG) emissions from the transportation sector have increased by 39% from 131 to 182 Mt of CO_2e as a consequence of the increase in population and the economy [2].

For rail transportation, the popular locomotive engine is an internal combustion engine operated by diesel fuel, which emits GHG emissions to the environment. Several studies have been conducted for alternative fuels and engines in order to reduce GHG emissions. For example, Hogerwaard and Dincer [3] have studied the effect of ammonia-ultra low sulfur diesel (NH_3-ULSD) duel fuel as an alternative replacement to the diesel fuel in a locomotive engine. Also, hydrogen production was added onboard to reuse the heat recovery from ammonia decomposition to reduce the diesel fuel consumption. They have found that heat recovery has improved the energy and exergy efficiencies for the new locomotive system. The alternative fuel has reduced the GHG emissions by 53% and the air contaminant emissions.

Marin et al. [4] conducted their research on the usage of hydrogen for passenger locomotives in the GO Transit Lakeshore corridor through Oshawa, Toronto, and Hamilton, in the province of Ontario in Canada. They compared three types of engines: diesel internal combustion engine, electrification, and hydrogen fuel cell. They found that the hydrogen fuel cell increased the weight of the electric locomotives by 30%, but it has higher flexibility and more economical than electrification. Their study has been extended to include energy supply and distribution. Marin et al. [5] have investigated the economic impact and flexibility of hydrogen production and distribution on the Bombardier ALP-46A locomotives. Four hydrogen production processes are included in their study: proton exchange membrane fuel cell, thermochemical Cu-Cl cycle, electrolysis, and steam methane reforming. They reported that the usage of hydrogen fuel cells has some drawbacks. The life expectancy of a fuel cell is one-third of that of diesel engines, and hydrogen storage at a higher energy density is less efficient than diesel on-board space utilization. Also, the implementation of fuel cells has an expected cost for high power transportation of 500 $/kW. Marin et al. [5] recommended internal combustion engines operating on hydrogen despite low efficiency to overcome the high operational cost of fuel cells.

https://doi.org/10.1016/j.fuel.2021.120529
Received 12 December 2020; Received in revised form 15 February 2021; Accepted 19 February 2021
Available online 31 March 2021

Nomenclature

Symbols

$\dot{E}x$	Exergy rate
h	specific enthalpy
$\dot{m}$	Mass flow rate
P	pressure
$\dot{Q}$	Heat transfer
r	Compression ratio
s	specific entropy
T	temperature
V	voltage
$\dot{W}$	Power

Subscript

ch	chemical
e	electric
en	energetic
eng	engine
ex	exergetic
ph	physical
th	thermal

Abbreviations

AF	Air-to-fuel ratio
ARS	Absorption refrigeration system
DME	Dimethyl ether
GT	gas turbine
ICE	Internal combustion engine
MCFC	molten carbonate fuel cell
NG	Natural gas
SR	Steam reforming
ULSD	ultra-low-sulfur diesel
WGS	Water gas shift

Greek Letters

η	Thermal efficiency
γ	Specific heat ratio
ν	Specific volume
ψ	Exergetic efficiency
ω	Specific fuel consumption

In order to reduce hydrogen consumption and increase the efficiency of fuel cells in locomotive engines, Hong et al. [6] constructed a small-scale locomotive system. The prototype locomotive comprises a proton exchange membrane fuel cell and a battery pack. They simulated different driving cycles and investigated the performance of the hybrid engine. They found that maintaining the charge state of the battery can achieve self-adaption function to improve efficiency by 2% and reduce the hydrogen consumption by 0.86 g. Similarly, Meegahawatte et al. [7] analyzed a hybrid fuel cell of commuter railway vehicles by analyzing power flow models of a hydrogen fuel cell stack, battery pack, and hybrid drive controller based on a typical return journey between Stratford Upon Avon and Birmingham in the United Kingdom. In addition, fuel consumption was compared among different types of engines, such as diesel engines and hybrid engines. They found that pure fuel cell engines can consume 38 kg of hydrogen for a long journey with a power of 355 kWh. However, the diesel-battery hybrid engine can consume 82 litres of diesel oil for a small journey with a power of 294 kWh. Also, the CO_2 emission was obtained from the hybridized fuel cell with a battery of 148.5 kg CO_2, which was the less amount compared to that of the diesel engine, diesel hybrid, and pure fuel cell engine.

In addition, Shinde et al. [8] performed the life cycle assessment for Mumbai Suburban Railway in India to include the construction and maintenance of railway infrastructures such as power supply installations, bridges, and platforms. It was found that the main contribution to the total environmental impact was the operation of the electric multiple units that feed the railway stations with electricity. The main reason for that was the dependence on power supply from conventional sources, such as charcoal and fossil fuels. To reduce GHG emissions, renewable energy sources should be considered in the operation phase. Moreover, Zhang et al. [9] investigated the proportion limit of coal power consumption for rail transit in 18 cities in China from 2015 to 2017. This investigation was performed in order to measure the carbon emission reduction in rail transit. They found that the environmental impact of rail transits is decreased compared to other transit modes due to the application of different sustainable strategies.

The specific objective of this paper is to propose a new powering system for locomotive transport, and investigate the performance of the proposed engine system based on thermodynamic analyses. In addition, the performance of the proposed engine system will be compared with traditional engines using alternative fuels. Furthermore, parametric studies for some operating conditions will be conducted.

2. System Description

The current rail-engine system is the R-Base, which is the baseline system as illustrated in Fig. 1. Air is compressed into the compressor of a turbocharger then flows to an aftercooled heat exchanger into the ICE at state point a3. A turbocharger turbine expands the exhaust of the ICE. It runs the compressor and delivers the remaining power to a starting generator. Other subsystems are included, which are the jacket water cooling and oil cooling subsystems. The fuel consumption is adjusted by the governor to control the engine speed. The current system is operated by ultra-low-sulfur diesel (ULSD) fuel. The ICE is connected to the generator to deliver the power to a traction motor, battery for storage, and auxiliary supplies. The engine model is selected based on the most common engine types in rail transportation sectors in the Canadian Provinces of Ontario and Quebec. It was found that the engine model, EMD 16–710-G3, is the most common engine that operates freight, passenger, and commuter trains in the two provinces. The specification and other technical details of the EMD 16–710-G3 are listed in Table 1.

A hybrid combined engine (R-1) is proposed, which consists of the ICE with a turbocharger and the gas turbine cycle combined with the molten carbonate fuel cell (MCFC), as shown in Fig. 1. The ICE and gas turbine (GT) are separate engines. The air is compressed in the turbocharger compressor and cooled down by the aftercooler heat exchanger before entering the ICE. Also, the fuel blend of hydrogen and hydroxyl is pumped to the ICE to be burnt with the compressed air in the pistons. The exhaust gas is released from the ICE entering the turbocharger turbine and used in the gas turbine system.

The GT consists of a compressor and a turbine is combined with a molten carbonate fuel cell (MCFC). Another amount of air is compressed, then cooled, expanded in the GT cycle, and used in the MCFC system. In the MCFC, the fuel is blended with water and exhaust gas from the ICE system and heated by that exhaust gas before entering the steam reforming (SR), the water gas shift (WGS), and then entering the anode of the MCFC.

Note that additional hydrogen gas may be added to the fuel stream before the MCFC. The anode flow exit enters a catalyst burner to burn the fuel with the expanded air from the turbine of GT, and the combustion results will enter the cathode to extract the carbon monoxide and carbon dioxide gases. Therefore, the exhaust gas has fewer carbon emissions and providing electric power from the MCFC. The excessive heat of the exhaust gas is utilized to produce cooling by an ammonia

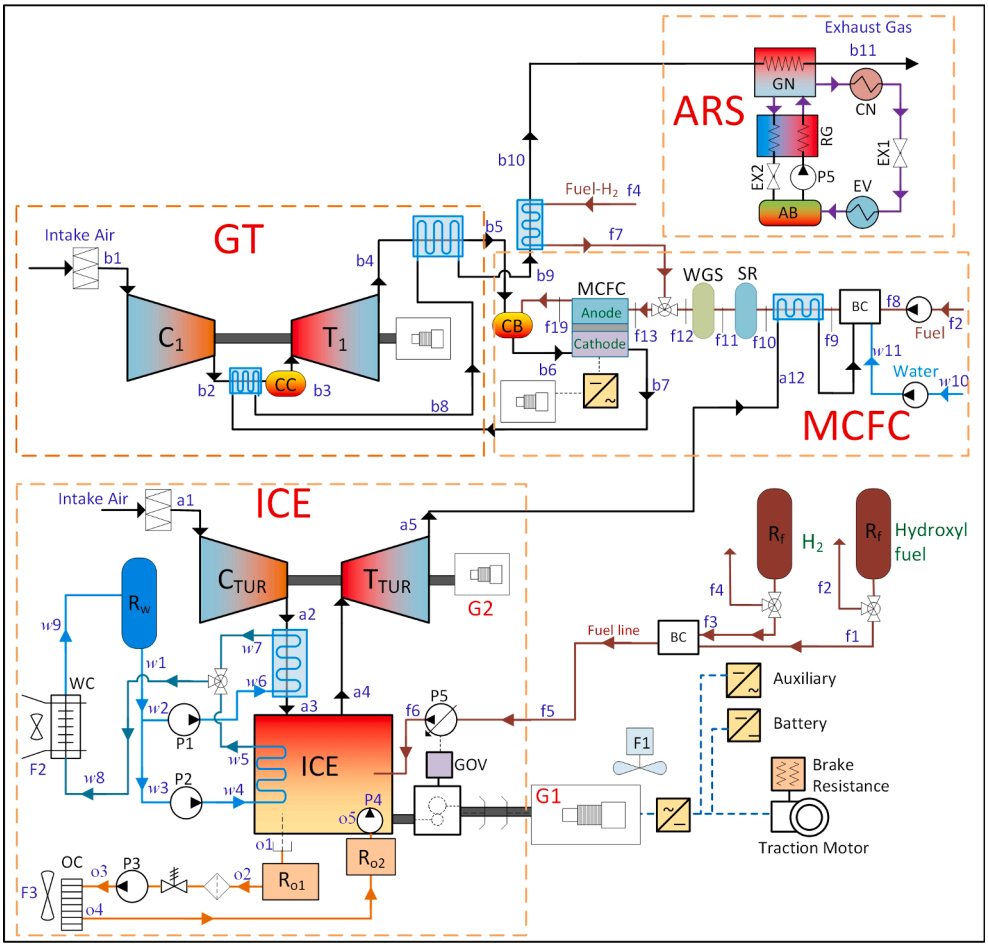

Fig. 1. The configuration of the proposed hybrid combined engine (R-1) system.

Table 1
Specifications of the locomotive engine.

Specifications	Values [10,11]	Units
Engine Model (EMD)	EMD 16-710G3	–
Engine Horsepower, EHP	4,500	hp
Engine Power, $\dot{W}_E$	3,355	kW
Output power per cylinder, $\dot{W}_{E\text{-}cy}$	210	kW
Engine Speed, N_{ICE1}	950	rpm
Brake mean effective pressure, b_{mep}	1,069	kPa
Displacement Volume per cylinder, V_d	11.635	l
Compression Ratio, r	15:1	—
Bore	0.23019	m
Stroke	0.2794	m
Number of cylinders, n_{cyl}	16	—
Fuel Tank Volume, V_{RES1}	8,410	l
Turbocharger Pressure Boost, ϕ_{TC}	1.25	—
Cooling water reservoir temperature, T_{RES3}	49	℃
Engine jacket cooling water outlet temp, T_{12}	85	℃
Maximum cylinder pressure, P_{max}	10,800	kPa

absorption refrigeration system. The net power is generated from the ICE, GT, and MCFC systems, which are connected to the generator to deliver the electric power to the traction motor and auxiliary systems. The excess electric power can also be stored in batteries.

3. Methodology

This chapter focuses on the thermodynamic analyses for the ICE, MCFC, GT, and ARS subsystems. The analyses are presented in detail below.

3.1. Thermodynamic analysis

The thermodynamic analysis is governed by the first and second law of thermodynamics and compare the developed system to the ideal case. The first law of thermodynamics is formulated by the conservation of mass and energy, while the second law of thermodynamics is formulated by the exergy balance equations. The used software programs in the analyses are the EES (Engineering Equation solver) and the Aspen-Plus software because of their reliable thermodynamic properties as well as the calculation methods and are extensively used by many researchers for thermodynamic analysis for several systems.

The thermodynamic balance equations can be expressed in general forms since the processes of each component are at steady-state equilibrium [12]. Therefore, the mass balance equation can be expressed as:

$$\sum \dot{m}_{in} = \sum \dot{m}_{out} \tag{1}$$

The general form of the energy balance equation in steady-state can be expressed as follows:

$$\sum_{in}\dot{Q}_{cv} + \sum_{in}\dot{W}_{cv} + \sum_{i}\dot{m}_i\left(h_i + \frac{1}{2}V_i^2 + gZ_i\right) = \sum_{out}\dot{Q}_{cv} + \sum_{out}\dot{W}_{cv} + \sum_{e}\dot{m}_e\left(h_e + \frac{1}{2}V_e^2 + gZ_e\right) \tag{2}$$

where $\dot{Q}_{cv}$ and $\dot{W}_{cv}$ represent the heat transfer and the work crossing the boundaries of a closed system of each component. The steady energy flow is expressed as $\left(h + \frac{1}{2}V^2 + gZ\right)$, which represents the internal energy of the media, the specific kinetic energy, and the specific potential

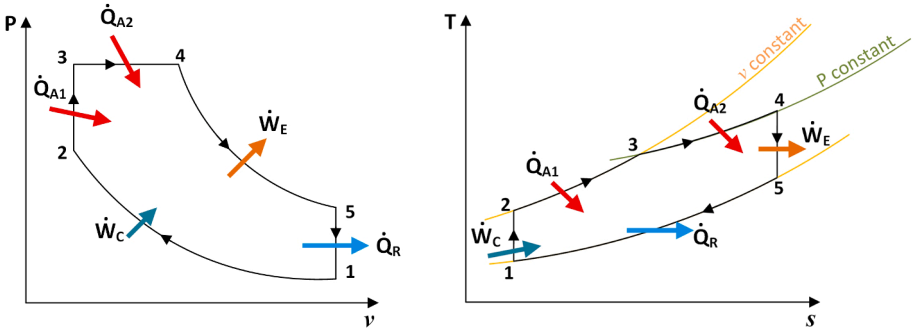

(a) P-*v* diagram (b) T-s diagram

Fig. 2. The P-v and T-s diagrams for the dual cycle without turbocharger.

energy, respectively. h is the specific enthalpy, V is the stream velocity of the working fluid, g is the gravitational acceleration, and Z is the elevation from the datum.

The general form of the second law of thermodynamics can be represented by the exergy balance equation in a steady-state condition for each process, and can be written as follows:

$$\sum_i \dot{m}_i ex_i + \sum_{in} \dot{E}x_Q + \sum_{in} \dot{E}x_W = \sum_e \dot{m}_e ex_e + \sum_{out} \dot{E}x_Q + \sum_{out} \dot{E}x_W + \dot{E}x_D \quad (3)$$

where $\dot{E}x_D$ refers to the exergy destruction rate, $\dot{E}x_W$ denotes the work done or required by the process, and $\dot{E}x_Q$ is thermal exergy due to the heat transfer within the boundaries ($\dot{Q}_{cv,i}$) and depends on the reference temperature T_o. They can be defined as follows:

$$\dot{E}x_W = \dot{W}_{cv} \quad \text{and} \quad \dot{E}x_{Q,i} = \left(1 - \frac{T_o}{T_{s,i}}\right)\dot{Q}_{cv,i} \quad (4)$$

The specific exergy of each stream is comprised of specific physical exergy, $\overline{ex}_{ph,i}$, and specific chemical exergy, $\overline{ex}_{ch,i}$, and are described as follows:

$$\overline{ex}_i = \overline{ex}_{ph,i} + \overline{ex}_{ch,i} = \sum_i \left[\left(\overline{h}_i - \overline{h}_o\right) - T_o(\overline{s}_i - \overline{s}_o)\right] + \sum_i n_i\left(\overline{g}_f^o + \overline{g}_{T_o} - \overline{g}^o\right) \quad (5)$$

The physical specific exergy depends on the specific enthalpy and entropy for a substance at specific temperature and pressure, while the chemical exergy depends on the chemical changes of a component composition during the chemical reactions. It depends on the Gibbs function of a unit mole of a substance $\overline{g}$, which consists of the Gibbs function of formation of each substance $\overline{g}_f^o$, Gibbs function of a substance at a specific temperature $\overline{g}_{T_o}$, and Gibbs function at a reference temperature $\overline{g}^o$.

3.2. Modeling of internal combustion engine

The prime locomotive mover is powered by a large two-stroke compression ignition (CI) diesel-fueled engine dual (limited pressure) cycle [13]. The ideal dual cycle consists of five processes: isentropic compression (1–2), heat addition (2–3) at constant volume, heat addition (3–4) at constant pressure, isentropic expansion (4–5), and constant volume heat rejection (5–1). The P-v diagram and T-s diagram for the ideal dual cycle without a turbocharger are illustrated in Fig. 2. The cycle model is developed according to the specification of the locomotive engine geometry and operating conditions like the compression ratio (r), cylinder volumes (V_i), rated traction power, and maximum cylinder pressure ($P_{max} = P_3$). The mass flow rate of air, $\dot{m}_a$ [13] drawn into the intake manifold is determined based on the engine geometry and rated operating conditions as:

$$\dot{m}_a = \eta_v\left(\frac{P_{in}\ V_d\ N_{ICE}\ n}{R_a T_{in}}\right) \quad (6)$$

where P_{in} and T_{in} are the pressure and temperature of the intake air to the ICE engine after the turbocharger, V_d is the total volume displacement of the ICE for all cylinders, R_a is the gas constant of air which is equivalent to 0.287 kJ/kg.K, N_{ICE} is the revolution of the engine speed [rpm] converted to [rev/s], n is the number of cylinders in the engine, and η_v is the volumetric efficiency, which is assumed to be 0.95. The equations describing the cycle processes are outlined in Table 2 for the ideal case with a constant specific heat ratio, $\gamma = 1.4$.

The heat addition, $\dot{Q}_A$, to the engine and the heat rejection, $\dot{Q}_R$, from the engine can be determined as follows:

$$\dot{Q}_A = \dot{Q}_{2-3} + \dot{Q}_{3-4} \quad \text{and} \quad \dot{Q}_R = \dot{Q}_{5-1} \quad (7)$$

The output power of the engine, including the turbocharger turbine and compressor, can be calculated as follows:

$$\dot{W}_{ICE} = \dot{W}_{1-2} + \dot{W}_{3-4} + \dot{W}_{4-5} + \dot{W}_{turbo,t} - \dot{W}_{turbo,c} \quad (8)$$

Table 2
The thermodynamic equations for the dual cycle processes.

Process	Description	P/T Relationship	Heat Equations	Work Equations
1 – 2	Isentropic compression	$P_2 = P_1 r^{\gamma}$ $T_2 = T_1 r^{(\gamma-1)}$	$\dot{Q}_{1-2} = 0$	$\dot{W}_{1-2} = \dot{m}_a \frac{P_1 v_1 - P_2 v_2}{(\gamma - 1)}$
2 – 3	Heat addition at constant volume	$\frac{T_3}{T_2} = \frac{P_3}{P_2}$	$\dot{Q}_{2-3} = \dot{m}_{ex} c_v (T_3 - T_2)$	$\dot{W}_{2-3} = 0$
3 – 4	Heat addition at constant pressure	$\frac{T_4}{T_3} = \frac{v_4}{v_3}$	$\dot{Q}_{3-4} = \dot{m}_{ex} c_p (T_4 - T_3)$	$\dot{W}_{3-4} = \dot{m}_{ex} P_3 (v_3 - v_4)$
4 – 5	Isentropic expansion	$P_5 = P_4\left(\frac{1}{r}\right)^{\gamma}$ $T_5 = T_4\left(\frac{1}{r}\right)^{(\gamma-1)}$	$\dot{Q}_{4-5} = 0$	$\dot{W}_{4-5} = \dot{m}_{ex} \frac{P_4 v_4 - P_5 v_5}{(\gamma - 1)}$
5 – 1	Heat rejection at constant volume	$\frac{T_5}{T_1} = \frac{P_5}{P_1}$	$\dot{Q}_{5-1} = \dot{m}_{ex} c_v (T_5 - T_1)$	$\dot{W}_{5-1} = 0$

The thermal efficiency, η_{ICE}, and the exergy efficiency, ψ_{ICE} of the internal combustion engine can be estimated as follows:

$$\eta_{ICE} = \frac{\dot{W}_{ICE}}{\dot{Q}_{ICE,add}} \quad \text{and} \quad \psi_{ICE} = \frac{\dot{W}_{ICE}}{\left(1 - \frac{T_a}{T_s}\right)\dot{Q}_{ICE,add}} \tag{9}$$

The indicated specific fuel consumption can be defined as:

$$\omega_f = \frac{\dot{m}_f \times 3600}{\dot{W}_{ICE}} \tag{10}$$

The chosen formula for ULSD is $C_{12}H_{24}$. The stoichiometric air–fuel (AF) ratio can be given according to the mass basis (AF_m) to be 14.77 kg_a/kg_f and molar basis (AF_M) to be 18 $kmol_a/kmol_f$.

3.3. Modeling of molten carbonate fuel cell

The MCFC employs molten salt electrolytes, which are made of eutectic mixtures of Li_2CO_3, Na_2CO_3, and K_2CO_3 [14]. The Li_2CO_3 (62 mol%) and K_2CO_3 (38 mol%) eutectic have been widely adopted [15]. These carbonates melt at approximately 500°C to allow transferring ions by the molten carbonates. The operating temperature should be at 923 K (650°C) to avoid the volatilization or solidification of the electrolyte. Therefore, the electrothermal reactions of the MCFC create electricity. The steam reforming (SR) and water gas shift (WGS) reactions occur sequentially to produce H_2 and CO in the MCFC stack [16]. The chemical reactions for SR, WGS, anode, and cathode are written as the followings:

- *SR* : $CH_4 + H_2O \rightarrow CO + 3\ H_2$ $\left(\Delta\bar{h}^0_{298K}\right) = 206$ kJ/mol
- WGS : $CO + H_2O \rightarrow CO_2 + H_2$ $\left(\Delta\bar{h}^0_{298K}\right) = -41$ kJ/mol
- *Anode* : $H_2 + CO_3^{2-} \leftrightarrow CO_2 + H_2O + 2e^-$
  $CO + CO_3^{2-} \leftrightarrow 2\ CO_2 + 2e^-$
- *Cathode* : $0.5\ O_2 + CO_2 + 2e^- \leftrightarrow CO_3^{2-}$
- *Overall* : $H_2 + 0.5\ O_2 + CO_2 \leftrightarrow H_2O + CO_2$ $\left(\Delta\bar{h}^0_{298K}\right) = 242$ kJ/mol

Note that the reforming reaction is a highly intensive endothermic process, while others are exothermic processes. Other reactions may occur at the anode, such as CO hydrogenation, methanation, and Boudouard reaction, and others may occur at the cathode, such as polycarbonate, peroxide, and superoxide [15]. After the electrochemical reactions, some byproducts, such as water and CO_2, whereas the excess air can be emitted from the cathode, as shown in Fig. 3. Here, CO_2 is consumed to form molten carbonates. Any unreacted fuels flow to the catalytic burner to be combusted with air, and its exhaust of carbon and oxygen gas flows to the cathode.

The electrochemical phenomenon of a unit fuel cell follows the governing equations. The cell voltage is estimated by the reversible potential taking into account the other losses: the Nernst loss, activation polarization, and concentration loss [17]. The cell voltage V_{cell} of the MCFC [V] can be expressed by:

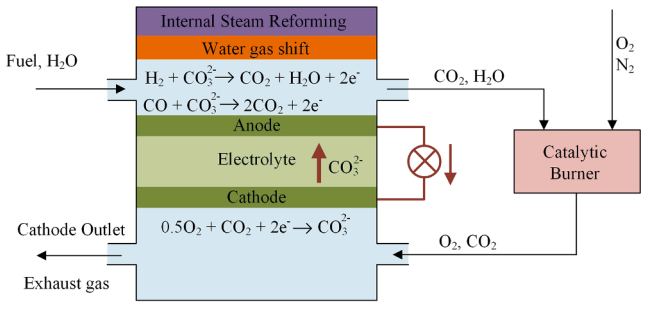

Fig. 3. The MCFC diagram with steam reforming and water gas shift.

$$V_{cell} = V^0 - V_{Nernst} - j(R_{an} + R_{ca} + R_{ohm}) \tag{11}$$

where V^0 is the reversible potential at standard conditions [V] and V_{Nernst} is the Nernst loss [V]. The maximum Nernst potential through can be fulfilled when the summation of V^0 and V_{Nernst} are considered through the electrochemical reaction. Also, the Nernst potential becomes the open-circuit voltage (OCV) when the current is zero. The j refers to the current density [mA/cm^2]. R_{an} and R_{ca} represent the activation losses of the anode and cathode [Ω −cm^2], respectively, to break the chemical bonds of H_2 and O_2 molecules in the electrochemical reaction, and R_{ohm} is the ohmic loss. The standard reversible potential is defined using the Gibbs free energy:

$$V^0 = -\frac{\Delta\bar{g}}{nF} \tag{12}$$

Where $V^0$is the Gibbs free energy [J/mol]; F is the Faraday constant, which is 96,485C/mol; and n is the molecular number of H_2; and $\Delta\bar{g}$ is function of the MCFC stack temperature [K].

$$\Delta\bar{g} = 0.002474T^2 + 48.996T - 243730 \tag{13}$$

The Nernst loss is a function of the concentrations of the substituents of the reactants and products:

$$V_{Nernst} = \frac{\bar{R}T}{nF}\ln\left(\frac{P_{H_2,an}\ P_{CO_2,an}}{P_{H_2,an}\ \sqrt{P_{O_2,ca}}\ P_{CO_2,ca}}\right) \tag{14}$$

where $\bar{R}$ is the molar gas constant, which is 8.314 J/mol.K, and P is the partial pressure at each electrode. The activation polarization losses that occurred in the anode and cathode are denoted as R_{an} and R_{ca}, which are modeled by Koh et al. [18].

$$R_{an} = 2.27 \times 10^{-5} \times \exp\left(\frac{\Delta\bar{h}_{an}}{\bar{R}T}\right) \times P_{H_2}^{-0.42}\ P_{CO_2}^{-0.17}\ P_{H_2O}^{-1.0} \tag{15}$$

$$R_{ca} = 7.505 \times 10^{-6} \times \exp\left(\frac{\Delta\bar{h}_{ca}}{\bar{R}T}\right) \times P_{O_2}^{-0.43}\ P_{CO_2}^{-0.09} \tag{16}$$

where $\Delta\bar{h}_{an}$ and $\Delta\bar{h}_{ca}$ are the activation energy values in the anode and cathode, respectively. The ohmic loss [Ω −cm^2] is the internal resistance due to the ionic and electronic conduction at the electrodes and the contacts. It can be calculated by the Arrhenius-type equation:

$$R_{ohm} = 0.5 \times \exp\left[3016\left(\frac{1}{T} - \frac{1}{923}\right)\right] \tag{17}$$

The net power output of an MCFC [W] is estimated as follows:

$$\dot{W}_{MCFC,AC} = jA_{cell}V_{cell}N\xi_{DC-AC} \tag{18}$$

where A_{cell} is the active area [cm^2], N is the number of the cells, ξ_{DC-AC} is the inverter efficiency to invert the direct current (DC) to alternating current (AC) and is equivalent to 0.95. The specifications of the MCFC are listed in Table 3.

The electric efficiency of MCFC can be determined as Eq. (19), while the thermal energetic and exergetic efficiencies can be evaluated as Eq.

Table 3
The specifications of MCFC.

Parameter	Value	Units
Operating temperature	923	K
Operating pressure	200	kPa
Current density, j	150	mA/cm^2
Anode activation energy, $\Delta\bar{h}_{an}$	53,500	J/mol
Cathode activation energy, $\Delta\bar{h}_{ca}$	77,300	J/mol
A_{cell}	6700	cm^2
N_{cell}	400 cells	—
N_{stack}	3 stacks	—

(20 and 21). The added heat of the MCFC, $\dot{Q}_{MCFC,add}$, is considered as the summation of the added heat through the anode, cathode, and the catalytic burner.

$$\eta_{MCFC,e} = \frac{\dot{W}_{MCFC,AC}}{\dot{W}_{MCFC,AC} + \dot{W}_{MCFC,loss}} \tag{19}$$

$$\eta_{MCFC,th} = \frac{\dot{W}_{MCFC,AC}}{\dot{Q}_{MCFC,add}} \tag{20}$$

$$\psi_{MCFC,th} = \frac{\dot{W}_{MCFC,AC}}{\dot{E}x^{Q}_{MCFC,add}} \tag{21}$$

3.4. Modeling of the gas turbine cycle

The gas turbine cycle consists of a compressor, heat exchanger, combustion chamber, and turbine. The net power of the gas turbine is determined to be:

$$\dot{W}_{GT} = \dot{W}_{T2} - \dot{W}_{C2} \tag{22}$$

The heat addition to the combustion chamber can be written as follows:

$$\dot{Q}_{CCGAS} = \dot{m}_{B4}h_{B4} - \dot{m}_{F}h_{F1} - \dot{m}_{B3}h_{B3} \tag{23}$$

The energetic and exergetic efficiencies are described as follows:

$$\eta_{GT} = \frac{\dot{W}_{GT}}{\dot{Q}_{CCGAS}} \quad \text{and} \quad \psi_{GT} = \frac{\dot{W}_{GT}}{\dot{E}x^{Q}_{CCGAS}} \tag{24}$$

3.5. Modeling of the absorption refrigeration system

The absorption refrigeration system is based on transferring the heating load into the cooling load [19]. It consists of a generator, condenser, evaporator, absorber, two expansion valves, and a pump. The working fluid is selected to be ammonia-water mixture. The mass balance, partial mass balance, and energy balance equations are presented in Table 4. The weak and strong solutions of ammonia are expressed by x_{ws} and x_{ss}, respectively. The pure solution of ammonia is expressed by x_{pure}. The energetic and exergetic COP of the cycle are described as:

$$COP_{en} = \frac{\dot{Q}_{AEV}}{\dot{Q}_{AGEN} + \dot{W}_{AP}} \quad \text{and} \quad COP_{ex} = \frac{\dot{E}x^{Q}_{AEV}}{\dot{E}x^{Q}_{AGEN} + \dot{W}_{AP}} \tag{25}$$

The overall performance of the rail engine system can be expressed by energetic and exergetic efficiencies as Eqs. (26) and (27). The useful energy sources are the net electric power of the MCFC, ICE, GT, pump, and the cooling load, while the required energy sources in the engine are the added heat of the ICE, GT, and endothermic heat of the steam reformer and water gas shift.

$$\eta_{eng} = \frac{\dot{W}_{MCFC,AC} + \dot{W}_{GT} + \dot{W}_{ICE} - \dot{W}_{p} + \dot{Q}_{cooling}}{\dot{Q}_{ICE,add} + \dot{Q}_{GT,add} + \dot{Q}_{SR} + \dot{Q}_{WGS}} \tag{26}$$

$$\eta_{eng} = \frac{\dot{W}_{MCFC,AC} + \dot{W}_{GT} + \dot{W}_{ICE} - \dot{W}_{p} + \dot{E}x^{Q}_{cooling}}{\dot{E}x^{Q}_{ICE,add} + \dot{E}x^{Q}_{GT,add} + \dot{E}x^{Q}_{SR} + \dot{E}x^{Q}_{WSG}} \tag{27}$$

3.6. Combustion modeling

The baseline fuel for the baseline system is the ultra-low-sulfur diesel (ULSD). The alternative fuels selected are hydrogen, methanol, and ethanol from monohydric alcohols, dimethyl-ether (DME) from ethers, and natural gas which is considered from hydrocarbons and presented as pure methane. Their properties are listed in Table 5. They are environmentally benign and have high ignition temperature, can be used in fuel cells and the ICE engines to provide power [20–23]. The Stoichiometric combustion reactions for the baseline fuels and alternative fuels are listed in Table 6. In this paper, five combinations of fuels are used in the study based on the mass fractions: F1 (75% natural gas and 25% hydrogen); F2 (75% methanol and 25% hydrogen); F3 (60% ethanol and 40% hydrogen); F4 (60% DME and 40% hydrogen); and F5 (15% natural gas, 40% hydrogen, 15% methanol, 15% ethanol, and 15% DME). The steam reforming, water gas shift, and catalytic burner for the five combination fuels are listed in Table 7.

4. Results and discussion

The hybrid combined locomotive engine is modeled using the Aspen plus. The equation of state is chosen to be the Soave-Redlick-Kwong (SRK) for the thermodynamic properties because it is the most widely accepted equation for modern chemical processes and recommended for gas mixtures and electrolytes (such as carbonate electrolyte CO_3^{2-}) at high temperature and pressure conditions [29–31]. Fig. 4 shows the Aspen flow chart for the ICE, MCFC, GT, and ARS subsystem. The MCFC subsystem is modeled using separate stoichiometric reactions for the anode and cathode, WGS, SR, and catalytic burner (CATBURN).

The absorption refrigeration system is illustrated in Fig. 4-b. The equation of state is selected to be the Peng-Robinson model, which has been recommended and used for refrigeration and liquefaction processes [31]. The exhaust gas is released to the environment after cooling down to 130°C. The released heat is used in the generator of the absorption refrigeration system to produce pure ammonia to the condenser and then to the evaporator. The absorber is modeled as decanter and the generator is modeled as the flash to produce the weak solution to the pump and strong solution from the generator to the expansion valve.

4.1. Thermodynamic analysis results

The thermodynamic results of the state points are listed in Table 8 for the hybrid combined engine and Table 10 for the absorption refrigeration system. Regarding the ICE system, the air mass flow rate enters the ICE at 3.26 kg/s, while the fuel mass flow rate is 0.15 kg/s. The air is

Table 4
The mass and energy balance equations for the absorption refrigeration system.

Component	Mass Balance	Partial Mass Balance	Energy Balance
ACOND	$\dot{m}_{A7} = \dot{m}_{A8}$	$x_{NH_3,A7} = x_{NH_3,A8} = x_{pure}$	$\dot{Q}_{ACOND} = \dot{m}_{A8}(h_{A7} - h_{A8})$
AEV	$\dot{m}_{A9} = \dot{m}_{A10}$	$x_{NH_3,A7} = x_{NH_3,A8} = x_{pure}$	$\dot{Q}_{AEV} = \dot{m}_{A9}(h_{A9} - h_{A10})$
AGEN	$\dot{m}_{A3} = \dot{m}_{A4} + \dot{m}_{A7}$	$\dot{m}_{A3}x_{NH_3,A3} = \dot{m}_{A4}x_{NH_3,A4} + \dot{m}_{A7}x_{NH_3,A7}$	$\dot{Q}_{AGEN} = \dot{m}_{A7}h_{A7} + \dot{m}_{A4}h_{A4} - \dot{m}_{A3}h_{A3}$
AHX	$\dot{m}_{A2} = \dot{m}_{A3}\dot{m}_{A4} = \dot{m}_{A5}$	$x_{NH_3,A2} = x_{NH_3,A3} = x_{ss}x_{NH_3,A4} = x_{NH_3,A5} = x_{ws}$	$\dot{Q}_{AHX} = \dot{m}_{A4}(h_{A4} - h_{A5})$
ABS	$\dot{m}_{A6} + \dot{m}_{A10} = \dot{m}_{A1}$	$\dot{m}_{A6}x_{NH_3,A6} + \dot{m}_{A10}x_{NH_3,A10} = \dot{m}_{A1}x_{NH_3,A1}$	$\dot{Q}_{ABS} = \dot{m}_{A6}h_{A6} + \dot{m}_{A10}h_{A10} - \dot{m}_{A1}h_{A1}$
AP	$\dot{m}_{A1} = \dot{m}_{A2}$	$x_{NH_3,A1} = x_{NH_3,A2} = x_{ss}$	$\dot{W}_{AP} = \dot{m}_{A1}(h_{A2} - h_{A1})$

Table 5
Specifications of alternative fuels for developed transportation systems.

Specifications	Hydrogen [24]	Methanol[25]	Ethanol[26]	DME[27]	NG[12]	ULSD[28]
Molecular formula	H_2	CH_3OH	CH_3OHCH_2	CH_3OCH_3	CH_4	$C_{12}H_{24}$
Molecular weight, M_i [kg/kmol]	2.016	46.069	46.07	46.07	16.043	168.3
Adiabatic flame temperature [°C]	2000	1949	2082	2100	1963	1977
Auto-ignition temperature [°C]	571	470	365	350	537	~ 225
Density at 40 °C [kg/m^3]	0.0773	792	789	2.11	0.657	876
Viscosity at 40 °C [mm^2/s]	109	0.75	1.056	0.184	18.72	4.1
High heating value [MJ/kg]	141.9	22.7	29.7	31.67	55.5	45.6
Low heating value [MJ/kg]	119.0	18.1	26.7	28.87	50	43.3

Table 6
The stoichiometric combustion reactions for the fuels.

Fuel	Stoichiometric combustion reaction	Heat of combustion (ΔH_c) [kJ/mol]
ULSD	$C_{12}H_{24} + 18\ O_2 \rightarrow 12\ CO_2 + 12\ H_2O$	−7674.5
Hydrogen	$2\ H_2 + O_2 \rightarrow 2\ H_2O$	−286
Methanol	$CH_3OH + 1.5\ O_2 \rightarrow CO_2 + 2\ H_2O$	−726
Ethanol	$CH_3OHCH_2 + 3\ O_2 \rightarrow 2\ CO_2 + 3\ H_2O$	−1366.91
DME	$CH_3OCH_3 + 3\ O_2 \rightarrow 2\ CO_2 + 3\ H_2O$	−2726.3
NG	$CH_4 + 2\ O_2 \rightarrow CO_2 + 2\ H_2O$	−891

pressurized through the compressor of the turbocharger from 101.3 to 126.63 kPa, then compressed by the piston to 4800 kPa. The air and fuel streams are heated in the combustion chamber at constant volume from 540.33℃ to 1150℃ and 9000 kPa. The combustion continues under constant pressure to 1350℃. The air is then expanded to 500 kPa and cooled to 350℃ and 340 kPa. The exhaust gas is expanded by the turbine of the turbocharger to the atmospheric pressure and 206℃. Regarding the gas turbine system, the air and fuel flow at 2.85 and 0.1 kg/s, respectively. The air is compressed from 101.3 kPa to 1500 kPa. The compressed air has a temperature of 430 ℃ and is heated to 630℃ by the HX1 and combusted with the fuel in CCGAS to increase its temperature to 980℃. The exhaust gas is expanded by the turbine to 100 kPa and 468℃. The exhaust gas is heated again by the heat exchanger HX2 before entering the catalytic burner. Table 9 shows the molar fraction of all state points due to the chemical reactions in the process.

For the MCFC system, the steam and the fuel enter the steam reformer (SR) and the water gas shift (WGS) at 0.06 kg/s and 0.1 kg/s, respectively. The SR has a temperature of 300℃, while the WGS has a temperature of 400℃. The anode, cathode, and CATBURN work at 650℃ and 200 kPa. The exhaust of the MCFC is released starting from B7 to B10 to the atmosphere after is has been cooled trice through the HX1, HX2, then COOLING. That excessive heat in the exhaust gas from the MCFC is used for heat recovery and increases the overall efficiency of the system.

The thermodynamic results of the absorption refrigeration system are shown in Table 10. The ammonia-water is pumped from A1 at 10℃ and 200 kPa to 2000 kPa. It is in a liquid state with a strong solution of 52.4% ammonia. Then it is heated by the regenerator heat exchanger (AHX) to 72 ℃ before entering the generator AGEN, which is heated to 125℃ to produce pure ammonia at state A7 (91.9% NH_3) and a weak solution at A4 (32.4% NH_3). The weak solution flows through the AHX then expanded through AEX2 to the absorber at 33 ℃ and 200 kPa. The pure ammonia is cooled down in the condenser at 60℃ then expanded by AEX1 to 200 kPa and heated through the evaporator AEV from −6.51℃ to 28℃.

The heat transfer and power of the components are presented in Table 11. The fuel used in this system is F1 (75% NG + 25% H_2). For the ICE turbocharger, the power of the compressor (TUR-C) and turbine (TUR-T) are 82.0 and 592.3 kW, while the thermal load of the after-cooling (AFTERCOOL) is 98.7 kW. The load of the ICE engine with the turbocharger is separately displayed in Table 12 to show the load of each process. The total net power of the ICE engine, including the turbocharger is 2569.2 kW and the added and rejected heat are 7833.5 and 1007.6 kW, as shown in Table 13. That engine has energetic and exergetic efficiencies of 32.8% and 41.48%, respectively. The gas turbine has a compressor power of 1217.6 kW and a turbine power of 1865.6 kW to produce a net power of 648.0 kW. It also needs a heating load of 2160.9 kW for the combustion of air and fuel, which has been reduced by using the heat exchanger recovery (HX1) with a duty of 631.8 kW. This GT system has energetic and exergetic efficiencies of about 30% and 40%, respectively.

The MCFC system is modeled with separate steam reforming and water gas shift units. The net power produced by the MCFC is 939.6 kW with a required heat of 1758.7 kW, 626.4 kW of SR and 58.1 kW of WGS. The electric and thermal efficiencies of the MCFC are 78.71% and

Table 7
The steam reforming, water gas shift and catalytic burner of MCFC system.

Fuels	SR	WGS	CB
F1	$CH_4 + H_2O \rightarrow CO + 3H_2$	$CO + H_2O \rightarrow CO_2 + H_2$	$CH_4 + 2O_2 \rightarrow CO_2 + 2H_2O$ $2H_2 + O_2 \rightarrow 2H_2O$ $CO + O_2 \rightarrow 2CO_2$
F2	$CH_3OH \rightarrow CO + 2H_2$	$CO + H_2O \rightarrow CO_2 + H_2$	$CH_3OH + 1.5O_2 \rightarrow CO_2 + 2H_2O$ $2H_2 + O_2 \rightarrow 2H_2O$ $CO + O_2 \rightarrow 2CO_2$
F3	$CH_3OHCH_2 \rightarrow CH_4 + CO + H_2$ $CH_4 + H_2O \rightarrow CO + 3H_2$	$CO + H_2O \rightarrow CO_2 + H_2$	$CH_3OHCH_2 + 3O_2 \rightarrow 2CO_2 + 3H_2O$ $2H_2 + O_2 \rightarrow 2H_2O$ $CO + O_2 \rightarrow 2CO_2$
F4	$CH_3OCH_3 \rightarrow CH_4 + CO + H_2$ $CH_4 + H_2O \rightarrow CO + 3H_2$	$CO + H_2O \rightarrow CO_2 + H_2$	$CH_3OCH_3 + 3O_2 \rightarrow 2CO_2 + 3H_2O$ $2H_2 + O_2 \rightarrow 2H_2O$ $CO + O_2 \rightarrow 2CO_2$
F5	$CH_4 + H_2O \rightarrow CO + 3H_2$ $CH_3OH \rightarrow CO + 2H_2$ $CH_3OHCH_2 \rightarrow CH_4 + CO + H_2$ $CH_3OCH_3 \rightarrow CH_4 + CO + H_2$	$CO + H_2O \rightarrow CO_2 + H_2$	$CH_4 + 2O_2 \rightarrow CO_2 + 2\ H_2O$ $CH_3OH + 1.5O_2 \rightarrow CO_2 + 2H_2O$ $CH_3OHCH_2 + 3O_2 \rightarrow 2CO_2 + 3H_2O$ $CH_3OCH_3 + 3O_2 \rightarrow 2CO_2 + 3H_2O$ $2H_2 + O_2 \rightarrow 2H_2O$ $CO + O_2 \rightarrow 2CO_2$

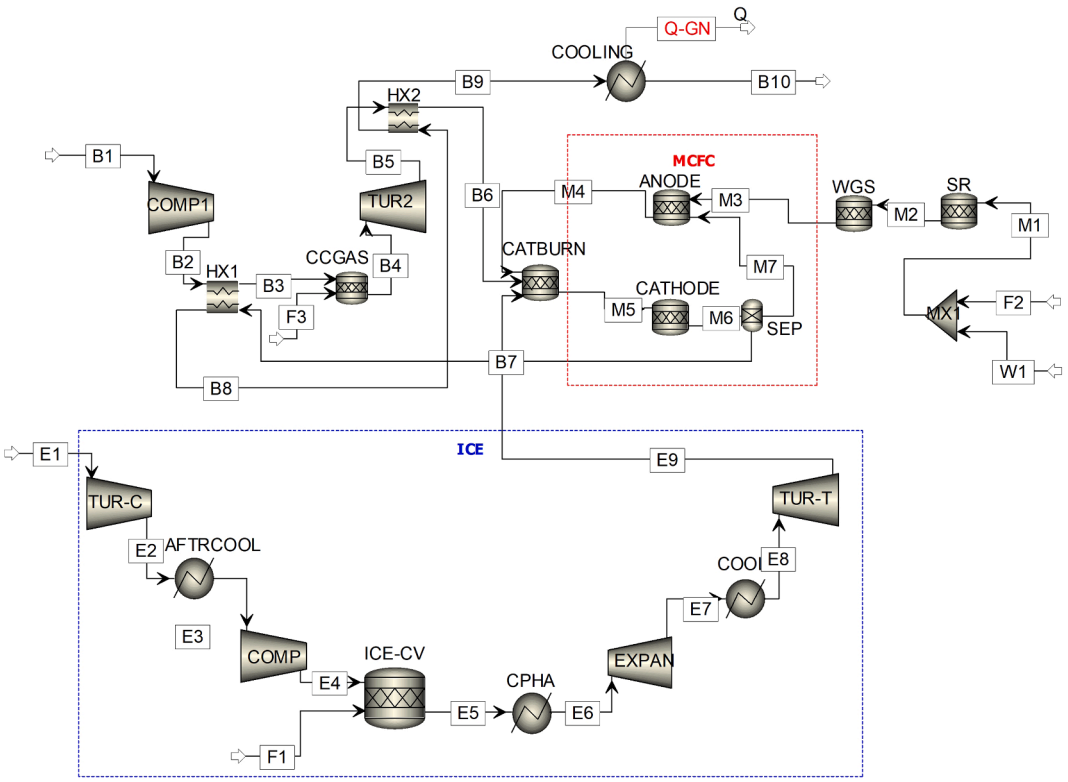

(a) The hybrid combined engine

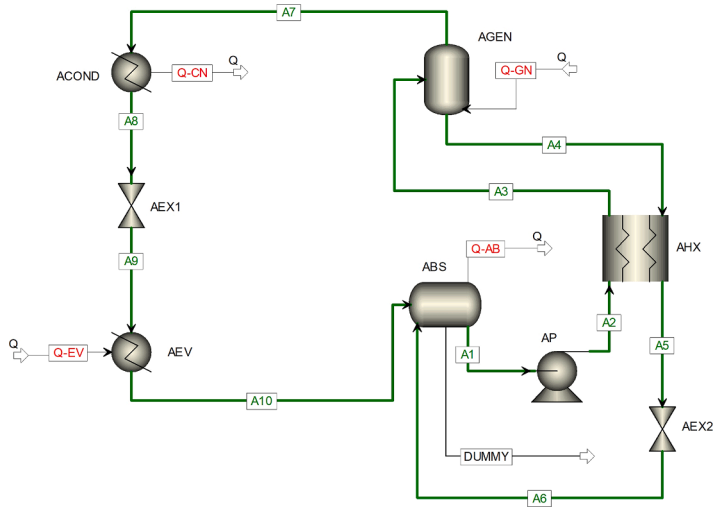

(b) The absorption refrigeration system.

Fig. 4. The Aspen flow chart for the hybrid combine engine with a refrigeration system.

53.43%, respectively. The exergy efficiency of the MCFC is 78.9%. The SR and WGS have 90% of thermal efficiency and above 75% exergy efficiency. For the absorption refrigeration system, the condenser and evaporator have a thermal load of 1215 and 615.1 kW, while the generator and absorber have a thermal load of 3346 and 2763 kW, respectively. The pump power is significantly small at 17.3 kW.

The performance of each subsystem and the overall system of the hybrid combined engine are presented in Table 13. The overall system has a net power of 4109.3 kW, which is composed of the ICE (2569.2 kW), GS (648 kW), MCFC (939.6 kW), and ARS (17.3 kW). The required heat for the hybrid engine is 10678.9 kW, combining all the required heat of all subsystems. The rejected heat includes that from the ICE, GC, and MCFC which are rejected to the environment, while the cooling load (615.1 kW) is included in the useful energy to the hybrid combined system. The overall energetic and exergetic efficiencies are 44.5% and 50.4%, respectively. As a result, combining the MCFC and GT with the ICE increases the overall net power by 61% and increases the overall heat required by 36% compared to that of the ICE. Also, the performance of the hybrid combined engine has been increased by 35% energetic efficiency and 25% exergetic efficiency compared to only the ICE engine.

4.2. Parametric studies

In this section, several parametric studies include the different fuels as mentioned in Section 3.1.3, the different operating pressures of the

Table 8
Thermodynamic properties of the state points for the hybrid combined engine using F1 (75%NG + 25%H_2) fuel.

State	$\dot{m}$[kg/s]	T[C]	P[kPa]	h[kJ/kg]	s [kJ/kg.K]	ex_{ph} [kJ/kg]	ex_{ch}[kJ/kg]	$\dot{E}x$[kW]
B1	2.85	20	101.3	−5.3	0.133	0.02	4.48	12.8
B2	2.85	430.27	1500	421.9	0.262	388.82	4.48	1120.9
B3	2.85	630.27	1500	643.6	0.539	527.89	4.48	1517.2
B4	2.91	980	1500	−184.7	0.937	899.52	154.35	3066.4
B5	2.91	468.0	100	−825.8	1.101	209.66	154.35	1059.3
B6	2.91	568.0	100	−706.0	1.252	284.24	154.35	1276.3
B7	6.20	650	200	−2372.8	0.928	515.62	78.46	3682.4
B8	6.20	575.5	200	−2474.8	0.813	448.01	78.46	3263.4
B9	6.20	533.7	200	−2531.0	0.745	412.04	78.46	3040.4
B10	6.20	135	200	−3040.4	−0.121	160.94	78.46	1483.9
E1	3.26	30	101.3	4.8	0.167	0.02	4.48	14.7
E2	3.26	54.86	126.63	30.0	0.182	20.55	4.48	81.6
E3	3.26	25	126.6	−0.3	0.085	19.11	4.48	76.9
E4	3.26	540.33	4800	545.0	0.085	564.38	4.48	1855.6
E5	3.41	1150	9000	−920.4	0.495	1310.68	46.44	4630.5
E6	3.41	1350	9000	−635.0	0.683	1540.13	46.44	5413.4
E7	3.41	568.45	500	−1708.9	0.683	466.19	46.44	1749.1
E8	3.41	350	340	−1978.3	0.432	271.77	46.44	1085.7
E9	3.41	206.07	101.3	−2147.5	0.496	83.38	46.44	442.9
F1	0.15	20	1000	−4441.3	−6.769	688.59	50103.7	7618.8
F2	0.1	20	101.3	−4058.1	−3.176	0.60	50103.7	5010.4
F3	0.06	20	2000	−4467.7	−7.535	890.71	50103.7	3059.7
M1	0.15	15.32	101.3	−11099.8	−6.364	−6.15	33841.0	5075.2
M2	0.15	300	200	−6924.1	2.299	895.77	34491.0	5308.0
M3	0.15	400	200	−6536.5	2.987	1151.74	34386.0	5330.7
M4	17.90	650	200	−803.1	−0.041	50.997	1528.65	28267.8
M5	24.22	650	200	−1020.4	0.360	153.0	1107.51	30525.7
M6	24.22	650	200	−642.1	0.233	130.83	1204.34	32333.9
M7	18.02	650	200	−46.9	−0.178	7.31	1643.05	29737.2
W1	0.1	20	101.3	−16058.4	−9.130	−3.05	527.33	52.4

Table 9
The mole fraction of chemicals in the hybrid combined system using F1 (75%NG + 25%H_2) fuel.

State	CO	CO_2	H_2O	H_2	O_2	N_2	CH_4	CO_3^{2-}
B1-B3	0	0	0	0	0.2166	0.7834	0	0
B4-B6	0	0.0239	0.1112	0.0070	0.1229	0.7322	0.0027	0
B7-B10	0	0.0247	0.2939	0	0	0.6814	0	0
E1-E4	0	0	0	0	0.2166	0.7834	0	0
E5-E9	0	0.0542	0.2524	0	0.0088	0.6846	0	0
M1	0	0	0.2212	0.7487	0	0	0.0301	0
M2	0.0257	0	0.1841	0.7873	0	0	0.0029	0
M3	0.0026	0.0231	0.1610	0.8105	0	0	0.0029	0
M4	0	0.0689	0.0798	0	0	0	0.0002	0.8511
M5	0	0.0576	0.1285	0	0.0234	0.2979	0	0.4927
M6	0	0.0111	0.1316	0	0	0.3050	0	0.5523
M7	0	0	0	0	0	0	0	1
W1	0	0	1	0	0	0	0	0

Table 10
Thermodynamic properties of the absorption refrigeration cycle.

State	$\dot{m}$[kg/s]	T[C]	P[kPa]	h [kJ/kg]	s [kJ/kg.K]	ex_{ph}[kJ/kg]	x_{NH_3}	x_{H_2O}	Q
A1	4.375	10	200	−9903.9	−10.494	44.61	0.524	0.476	0
A2	4.375	10.31	2000	−9900.6	−10.491	47.10	0.524	0.476	0
A3	4.375	72.31	2000	−9608.1	−9.559	61.72	0.524	0.476	0
A4	2.903	125	2000	−11747	−8.509	71.58	0.324	0.676	0
A5	2.903	32.92	2000	−12187.8	−9.767	5.38	0.324	0.676	0
A6	2.903	33.23	200	−12187.8	−9.758	3.05	0.324	0.676	0.042
A7	1.472	125	2000	−3403.3	−6.318	448.40	0.919	0.081	1
A8	1.472	60	2000	−4125.3	−8.320	322.90	0.919	0.081	0.613
A9	1.472	−6.51	200	−4125.3	−7.594	106.61	0.919	0.081	0.766
A10	1.472	28	200	−3826.6	−6.527	87.41	0.9189	0.081	0.917

MCFC, and the maximum pressure levels of the GT.

4.2.1. Effect of different fuels

In this paper, five fuels as natural gas as methane, methanol, ethanol, and dimethyl ether, and hydrogen are selected beside the ULSD diesel fuel. The fuels are combined with hydrogen in different ratios based on the molar fraction of CO_2, O_2, H_2 and H_2O in the anode and cathode in the MCFC, yielding to the partial pressure of these substituents to produce high power with maximum electric efficiency, which is discussed later.

Table 11
The energy loads and efficiencies of components using F1 (75%NG + 25%H_2) fuel.

Component	$\dot{Q}$[kW]	$\dot{W}$[kW]	$\dot{E}x_D$[kW]	η [%]	ψ [%]
ICE-turbocharger					
TUR-C	0	82.0	15.0	80	81.68
AFTRCOOL	98.7	0	3.1	100	34.71
TUR-T	0	592.3	66.6	85	88.76
GT System					
COMP1	0	1217.6	109.5	80	91.01
HX1	631.8	0	23.2	100	99.54
CCGAS	2160.9	0	4246.7	90	41.93
TUR1	0	1865.6	141.9	85	92.39
MCFC system					
MCFC	1758.7	939.6	1965.5	78.71_{e}, 53.43_{th}	78.90
SR	626.4	0	67.8	90	77.44
WGS	58.1	0	9.7	90	99.82
Heat recovery heat exchangers					
COOLING	3358.7	0	787.9	100	52.62
HX2	348.5	0	5.9	100	99.86
ARS system					
ACOND	1215.0	0	83.5	100	88.94
AEV	615.1	0	132.8	100	1.99
AHX	1462.5	0	146.4	100	69.03
AGEN	3346.0	0	157.4	100	81.28
ABS	2763.0	0	170.0	100	21.72
AP	0	17.3	4.2	70	75.97

Table 12
The ICE engine performance using F1 (75%NG + 25%H_2) fuel.

Description		Aspen block name	$\dot{Q}$[kW]	$\dot{W}$[kW]
1–2	Isentropic compression	COMP	0	1778.7
2–3	Heat addition at constant volume	ICE-CV	6812.2	0
3–4	Heat addition at constant pressure	CPHA	1021.4	63.0
4–5	Isentropic expansion	EXPAN	0	3774.5
5–1	Heat rejection at constant volume	COOL	1007.7	0

Table 13
The hybrid combined engine performance using F1 (75%NG + 25%H_2) fuel.

Subsystem	$\dot{W}$[kW]	$\dot{Q}_{add}$[kW]	$\dot{Q}_{rej}$[kW]	η [%]	ψ [%]
ICE	2569.2	7833.5	1106.4	32.8	40.17
GC	648.0	2160.9	0.00	29.99	39.4
MCFC	939.6	0.00	564.8	78.71_{e} & 26.0_{th}	78.9
SR	0.00	626.4	0.00	90	77.44
WGS	0.00	58.1	0.00	90	99.82
ARS	17.3	0.00	615.1	18.29	9.54
Entire System	4139.6	10678.9	615.1	44.52	50.4

The effect of fuels with the different combinations is studied in all systems. The ICE engine is the main prime mover in the trains and it works using fossil fuels, which have a negative impact on the environment. Therefore, the performance of the ICE engine is compared with respect to fuel types, as shown in Table 14. The net power of the ICE has been increased for all alternative fuels compared to ULSD (2172 kW). The added heat in the combustion is also increased using the alternative fuels compared to ULSD (4671.2 kW). The highest required heat is 7833.5 kW for F1 (methane and hydrogen). The minimum required heat is used for combining methanol and hydrogen (4576.9 kW). Therefore, the thermal and exergy efficiency of the ULSD ICE engine are 46.5 and 57%, respectively. The highest performance of the ICE engine under the same operating conditions and flow rates is using F2 (75% methanol and 25% hydrogen). The remaining fuels (F1, F4, and F5) have similar thermal and exergy efficiency of about 35% and 41%, respectively, which are less than that of the ULSD.

The effect of the fuels on the performance of the gas turbine system is studied, and the results are shown in Table 15. The maximum required heat in the combustion chamber is 2160.9 kW for F1 fuel, while the minimum required heat is 991.6 for F2. However, the maximum and minimum net power are 669.8 kW for F5 and 627.6 kW for F2. As a result, the maximum and minimum energetic and exergetic efficiencies are about 63% and 83% for F2 and 30% and 40% for F1, respectively.

In addition, the effect of the fuels on the MCFC performance is investigated, as displayed in Table 16. The loss voltage is the summation of the activation losses of the anode and cathode and the ohmic loss. The cell voltage is the difference between the standard reversible potential and Nernst loss and activation. The highest loss voltage is 0.222 V for F1, while the minimum is 0.181 V for F2. Similarly, the maximum and minimum cell voltage is 0.851 and 0.818 V for F2 and F5, respectively. Hence, the cell power is the maximum of 939.6 kW for F1 and the minimum of 937.1 kW for F5. The required heat for the MCFC has a range of 1760 kW for F1 to 5215 kW for F2. Consequently, the maximum and minimum thermal and exergetic efficiencies are about 53% and 79%

Table 15
Gas turbine performance with respect to different fuels.

Parameter	F1	F2	F3	F4	F5
$\dot{Q}_{CCGAS}$[kW]	2160.9	991.6	1949.6	2018.9	2091.1
$\dot{W}_{GT,net}$[kW]	648.0	627.6	665.2	665.2	669.8
η_{GT}[%]	29.99	63.29	34.12	32.95	32.03
ψ_{GT}[%]	39.35	83.04	44.77	43.83	42.61

Table 16
The MCFC performance with respect to different fuels.

Parameter	F1	F2	F3	F4	F5
V_{loss}[V]	0.222	0.181	0.193	0.193	0.188
V_{cell}[V]	0.820	0.851	0.822	0.824	0.818
$\dot{W}_{MCFC,AC}$[kW]	939.6	974.9	942.0	943.7	937.1
$\dot{W}_{MCFC,loss}$[kW]	254.2	207.5	221.0	221.2	214.8
$\eta_{MCFC,e}$[%]	78.71	82.45	80.99	81.01	81.35
$\dot{Q}_{MCFC,add}$[kW]	1758.7	5215.4	2414.3	2430.5	2460.7
$\dot{Q}_{MCFC,loss}$[kW]	564.8	4033.0	1251.2	1265.7	1308.8
$\eta_{MCFC,th}$[%]	53.43	18.69	39.02	38.83	38.08
$\psi_{MCFC,th}$[%]	78.90	27.61	57.62	57.34	56.24

Table 14
ICE performance with respect to different fuels.

Parameter	ULSD	F1	F2	F3	F4	F5
$\dot{W}_{ICE}$[kW]	2172	2569.2	2477.4	2640.7	2640.7	2660.3
$\dot{Q}_{ICE,add}$[kW]	4671.2	7833.5	4576.9	7276.7	7456.4	7672.0
$\dot{Q}_{ICE,rej}$[kW]	968.9	1106.4	1004.1	1092.46	1092.5	1105.1
$\dot{E}x_{ICE,des}$[kW]	8033.3	13131.8	7325.8	12052.9	12169.3	12611.1
η_{ICE}[%]	46.5	32.80	54.13	36.29	35.42	34.68
ψ_{ICE}[%]	57.0	40.17	63.08	42.29	41.27	42.48

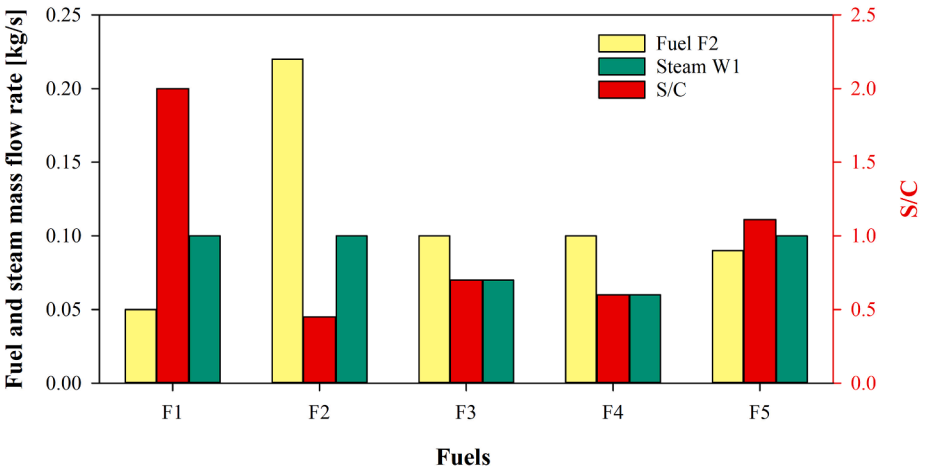

Fig. 5. The fuel and steam mass flow rate entering the SR and the S/C ratio.

Table 17
Molar fraction of substituents on anode and cathode of MCFC.

Substituent	F1	F2	F3	F4	F5
Anode					
x_{H_2}	0.8105	0.8618	0.8062	0.8229	0.8016
x_{CO_2}	0.0689	0.1285	0.1200	0.1204	0.1429
x_{H_2O}	0.0798	0.1181	0.1280	0.1255	0.1513
Cathode					
x_{O_2}	0.0234	0.0419	0.0325	0.0326	0.0341
x_{CO_2}	0.0576	0.0870	0.0699	0.0700	0.0757

Table 18
The absorption Refrigeration system performance with respect to fuels.

Parameter	F1	F2	F3	F4	F5
$\dot{Q}_{AGEN}$ [kW]	3346.0	3218.9	2944.5	2944.5	2927.8
$\dot{Q}_{AEV}$ [kW]	615.1	483.6	442.3	442.3	439.8
$\dot{Q}_{ABS}$ [kW]	2763.0	2549.3	2332.0	2332.0	2318.8
$\dot{Q}_{ACON}$ [kW]	1215.01	1168.8	1069.2	1069.2	1063.1
$\dot{W}_{AP}$ [kW]	17.26	15.73	14.39	14.39	14.30
COP_{en} [%]	18.29	14.95	14.95	14.95	14.95
COP_{ex} [%]	9.54	7.80	7.8	7.8	7.8
$\dot{m}_{ABS}$ [kg/s]	5	4.81	4.4	4.4	4.375

.

for F1 and 18% and 27%, respectively.

The fuel and steam flow rates entering the MCFC are different for each fuel type as shown in Fig. 5. The S/C refers to the steam to carbon ratio, which is equivalent to the steam to fuel ratio. The steam flow rate at state point (W1) has two values of 0.1 kg/s for F1, F2, and F5 fuels and 0.07 kg/s for F3 and 0.06 kg/s for F4. However, the fuel flow rates are 0.05 kg/s for F1, 0.09 kg/s for F5, 0.1 kg/s for F3 and F4, and 0.22 kg/s for F2. Accordingly, the S/C is the highest of 0.2 for F2 and the lowest of 0.04 for F2. These values of mass flow rates are chosen to avoid the resulting error in modeling the MCFC using Aspen Plus and to maintain the molar fraction of the substituents in the anode and cathode reactions, as shown in Table 17. The molar fraction of hydrogen in the anode should be above 0.8, while the carbon dioxide and steam are slightly above 0.1. however, the molar fraction of oxygen in the cathode is about 0.03 and above 0.05 to 0.08. These molar fraction values have a significant impact on Nernst loss potential, the activation loss in the anode and cathode since they are a function of partial pressures for H_2, CO_2, O_2, and H_2O in the anode and cathode plate.

Furthermore, the effect of fuels on the absorption refrigeration system is considered as illustrated in Table 18. The exhaust temperature should be cooled to 130℃ B10, and the heat rejected is used to increase the generator temperature to 125℃. The heating loads of the generator vary from 2917.8 kW for F5 to 3346 kW for F1. However, the cooling loads have a range from 439.8 kW for F5 to 615 kW for F1. The resulting COP_{en} is about 15% except for F1 where it is 18%, while the COP_{ex} is about 7.8% and 9.5% for F1. The mass flow rates of ammonia pumped in State A1 are different to suit the generator load.

The net power for the subsystems and overall system using different fuels are illustrated in Fig. 6-a. The overall net power is increased to more than 4000 kW for all fuels compared to 2000 kW of the traditional ICE. The specific fuel consumption is displayed in Fig. 6-b to show the ratio of the fuel mass flow rate to the net power of the system. The traditional ICE has 0.25 kg/kWh for ULSD fuel. However, the GT and MCFC have an average value of 0.32 and 0.35 kg/kWh using the ULSD fuel, respectively. The hybrid combined system has different values slightly changing from 0.25 and a maximum of 0.39 kg/kWh for F2 fuel. Using F1 fuel reduced the specific fuel consumption to 0.24 kg/kWh for the whole engine. The overall thermal and exergy efficiencies are similar in values of about 43% and 50%, respectively, for all fuels except F2 (methanol and hydrogen) which has 68% thermal efficiency and 82% exergetic efficiency, as shown in Fig. 7-a. However, the CO_2 emissions from the ICE using diesel fuel is the most significant of 0.45 kg/s. Using alternative fuels dropped this value by about 30% for F1 and 50% for fuels F2 to F5. The GT system produces less emissions of an average of 0.05 kg/s, as shown in Fig. 7-b. The emissions from the MCFC is composed of the chemical reactions in the anode, cathode, SR, and WGS, as well as the emissions from the ICE and GT. Therefore, the emission of the MCFC has values of less than 0.1 kg/s for fuels F2 to F4, 0.15 kg/s for F5, and 0.27 kg/s for F1. That means a total reduction of 60% can be achieved using F2, while 65% F3 and F4 fuels.

4.2.2. *Effect of pressure on the MCFC performance*

The working pressure of the MCFC is studied with respect to the power and efficiency under a condition of maintaining the operating temperature at 650℃. Fig. 8 presented the change in output power and the electric efficiency. As observed, increasing the pressure from 100 to 1000 kPa increases the output power from 800 kW to 1100 kW and correspondingly increases the electric efficiency from 75% to 90%. However, increasing the pressure raises the thermal efficiency to its maximum at 200 kPa then gradually decreases to the minimum value for each fuel type. In addition, the exergetic efficiency shows similar trends as the thermal efficiency shown in Fig. 9. The net power was gained by using F3 fuel, but the highest thermal and exergetic efficiency were obtained by F5 fuel. This is due to the increase in the required heat for

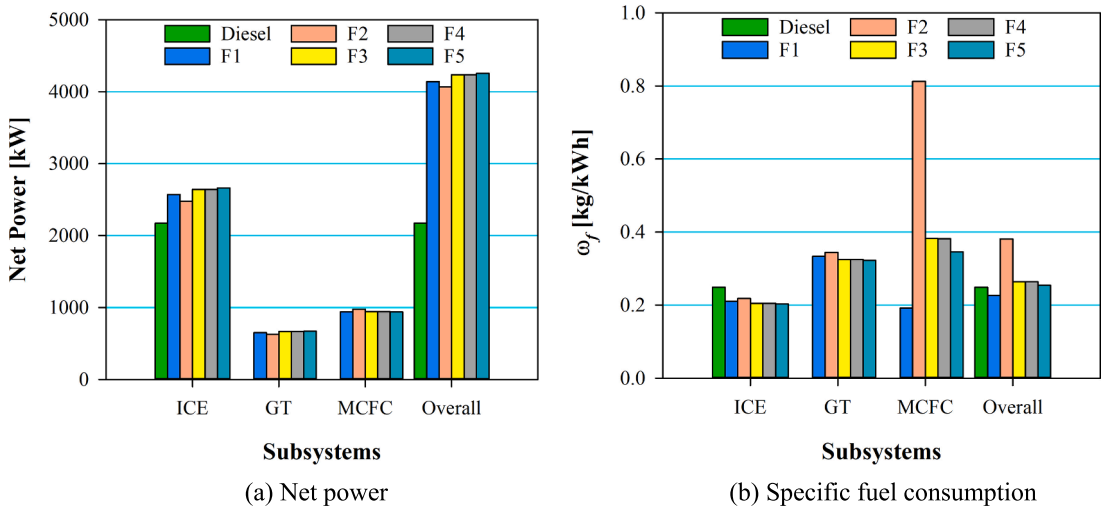

Fig. 6. The net power and specific fuel consumption for the subsystems and overall system.

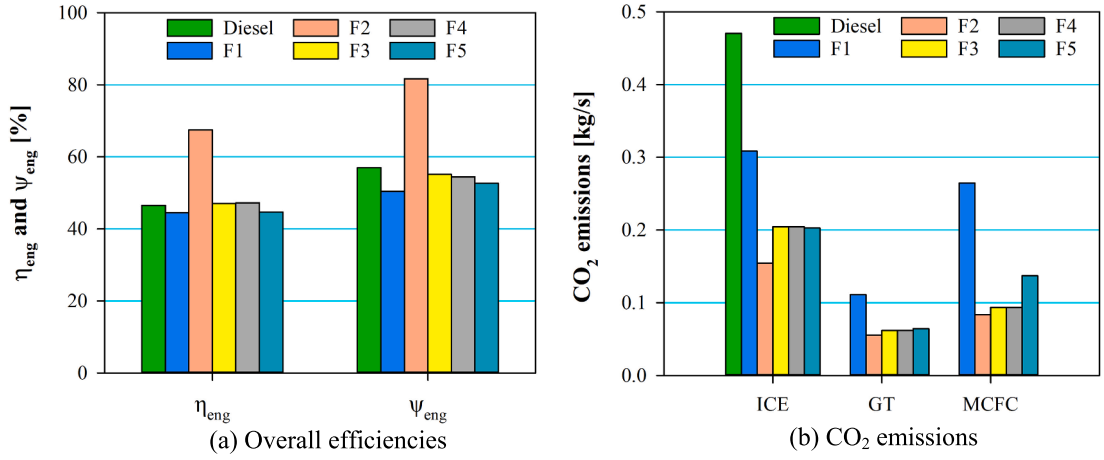

Fig. 7. The overall efficiencies for the overall system and the CO_2 emissions for the subsystems.

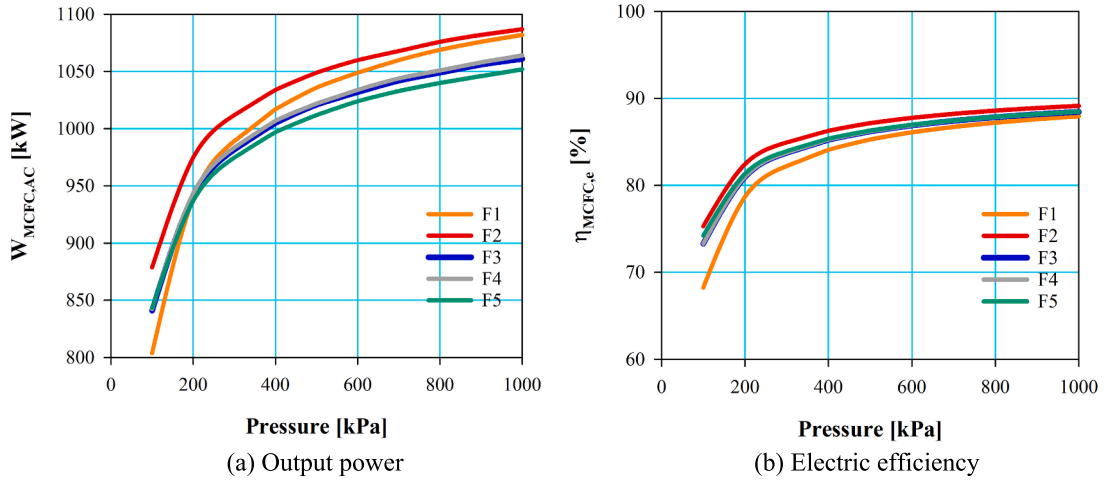

Fig. 8. The output power and electric efficiency for the MCFC using different fuels.

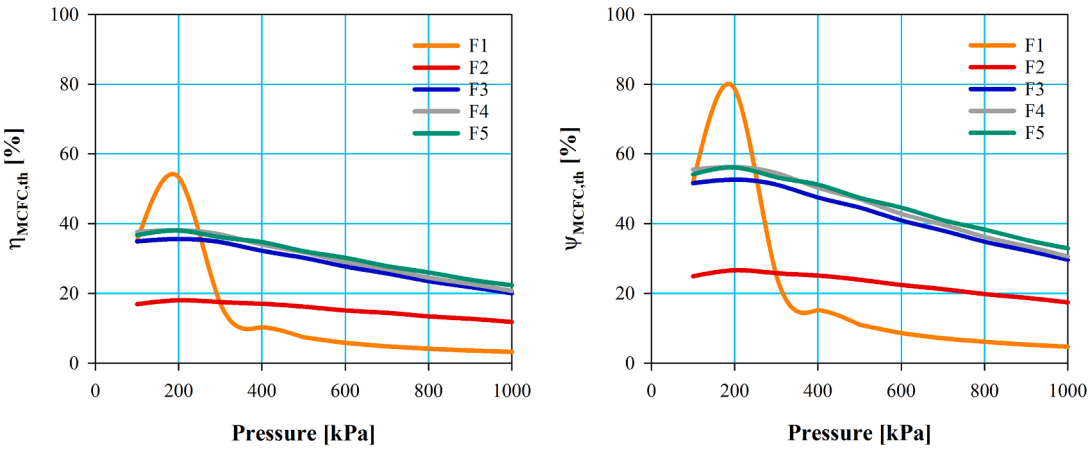

(a) Energetic efficiency (b) Exergetic efficiency

Fig. 9. The energetic and exergetic efficiencies of the MCFC using different fuels.

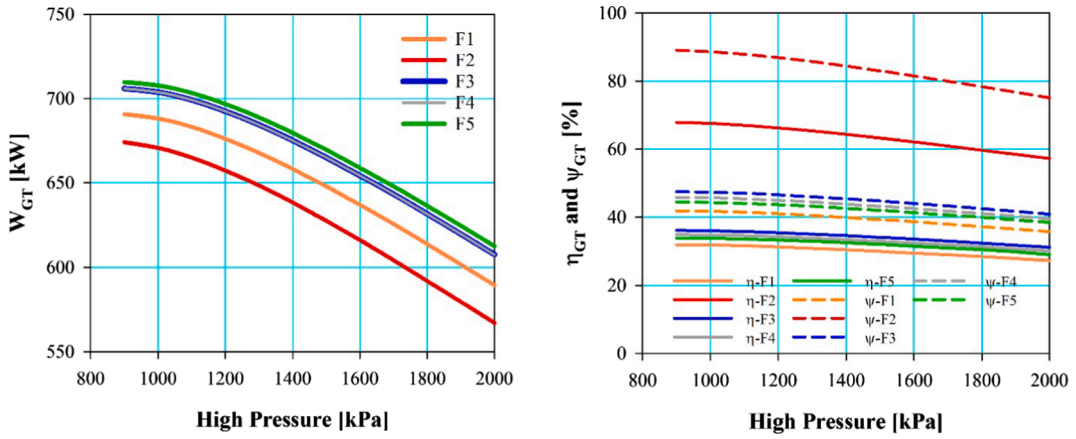

(a) Net power (b) Energetic and exergetic efficiencies

Fig. 10. The net power and energetic and exergetic efficiencies of GT using different fuels.

chemical reactions in the anode, cathode, and catalytic burner. Therefore, the best operating pressure is 200 kPa to produce high output power with high electric, thermal, and exergetic efficiencies for all alternative fuels.

4.2.3. Effect of high pressure on the GT performance

High pressure has an interesting role in the GT performance, as shown in Fig. 10. Two conditions hold for the analysis, including the output temperature of the heat exchanger (HX1) at B3 to be 630℃ because of the constant operating temperature of the MCFC as it is linked to the HX1 and the output temperature of combustion for the turbine safety at 980℃. Therefore, increasing the high pressure of the GT significantly decreases the net power of the system from 700 to 550 kW. Consequently, it slightly decreases the thermal efficiency from 35% to 28% and exergetic efficiency from 45 to 40%. The maximum net power can be accomplished using the combination of all fuels as in F5, while the minimum power can be fulfilled using F2 of methanol and hydrogen fuel mixture for all the pressure range. The decrease in net power is due to the combination of a significant increase in the compressor power compared to a gentle increase in turbine power.

In addition, the decrease in the efficiencies is because of increasing the combustion heat due to the increase of pressure, as shown in Fig. 10-b. At 900 kPa, the thermal and exergetic efficiencies are 31.9% and 41.9% for F1, 67.9% and 89.1% for F2, 36.2% and 47.5% for F3, 34.9% and 45.8% for F4, and 33.9% and 44.5% for F5, respectively. At 2000 kPa, the thermal and exergetic efficiencies decrease to 27.3% and 35.8% for F1, 57.3% to 75.1% for F2, 31.2% and 40.9% for F3, 30.1% and 39.5% for F4, and 29.3% and 38.3% for F5, respectively. In previous analyses, the GT was modeled at a high pressure of 1500 kPa, which produced a net power of an average of 650 kW, which was not the best choice. Therefore, the best operating high pressure of the system is at 900 kPa to increase the net power to 700 kW and increase the thermal efficiency to 35%.

The hybrid combined locomotive engine has many components but it can be technically applied and compatible. According to the net power of each subsystem, the weight of the ICE is 18,000 kg, which is given in the specification of EMD 16–710-G3 in Table 1. The weight of the MCFC is estimated to be 10,330 kg, as 10 kg/kW [15], which is about 57% of the ICE. Also, the weight of the GT is evaluated to be 600 kg about 3% of the ICE [32]. In addition, the weight of ABS is 4816 kg about 27% of the ICE [33]. That means the weights of all subsystems are 33,746 kg which is doubled the weight of the ICE. The current hood unit has the ICE unit and fuel storage tank, but it can be modified and extended to include the subsystems. The MCFC stacks can be distributed at the rooftop of the hood unit, and the GT engine has the smaller weight and size to be placed as the behind the ICE. The ARS is placed at the end of hood unit since its generator is connected to the exhaust gases of the three subsystems. The condenser can be exposed to the outside of the unit which can be cooled by the outside, high-speed, moving air. The evaporators can be distributed at the top of other fleet units to provide the required

cooling loads. In addition, the fuel storage tanks can be located at the end of a hood unit and stacked. It is preferable to use liquid phases to reduce the tank sizes.

5. Conclusions

This paper presents an investigation of the performance of a proposed hybrid combined locomotive engine using five alternative fuels with different combinations. The proposed locomotive engine system consists of the ICE, GT, and MCFC, in addition to an absorption system. Thus, the main output from this system are electric power and cooling loads for air conditioning the trains. The alternative fuels are natural gas, methanol, ethanol, hydrogen, and dimethyl ether, and different combinations of them. A number of points can be concluded from this study, as follows:

- The utilization of alternative fuels increases theoutput power compared to the fossil fuel in the ICE engine by 25%. Also, the net power of the ICE using different fuels has increased fourfold of that of the GT and threefold of that of the MCFC.
- The proposed hybrid combined engine system has doubled the net power of the GT to 4200 kW with less specific fuel consumption.
- The overall efficiency of the hybrid combined system is about 43% and 55% thermal and exergetic efficiencies, respectively. The highest performance can be obtained using the fuel with the mass fractions of 75% methanol and 25% hydrogen. The performance can reach 68% thermal efficiency and 82% exergetic efficiency.
- The alternative fuels used produced 65% reduction in emissions., The minimum environmental impact can be achieved by the fuel with 75% methanol and 25% hydrogen at less than 0.08 kg/s.
- Combining all the alternative fuels as in F5 produced slightly high emissions about 0.15 kg/sCO_2 eq. However, it has less specific fuel consumption of 0.25 kg/kWh and produced high power of 4250 kW.
- Increasing the operating pressure from 100 to 1000 kPa can increase the net power of the MCFC from 800 to 1100 kW and its electric efficiency from 70 to 90%. However, it decreases the thermal efficiency from 38% to 20% and the exergetic efficiency from 40 to 30%. The best operating pressure is at 200 kPa because of the maximum thermal and exergetic efficiencies and high electric performance.
- Increasing the high pressure of the GT system leads to a gradual decrease of the thermal and electric performances. The net power decreases from 700 kW to 550 kW with a gradual decline to 25% and 40% in thermal and exergetic efficiencies, respectively. The best performance should be at 900 kPa to produce 700 kW.

Finally, the proposed hybrid combined engine system reported in this paper provides clean rail transportation. It is considered an eco-friendly approach to produce electric power using alternative fuels to enhance environmental sustainability. Further analyses will be performed in the near future focusing on multi-objective optimization, exergoenvironmental, and exergoeconomic analyses for a more comprehensive assessment of the proposed system for practical applications.

CRediT authorship contribution statement

Shaimaa Seyam: Methodology, Software, Data curation, Writing - original draft, Investigation, Visualization, Writing - review & editing. **Ibrahim Dincer:** Supervision, Conceptualization, Funding acquisition, Writing - review & editing. **Martin Agelin-Chaab:** Supervision, Conceptualization, Funding acquisition, Writing - review & editing.

Declaration of Competing Interest

The authors declare that they have no known competing financial interests or personal relationships that could have appeared to influence the work reported in this paper.

Acknowledgement

The support of this research by the Natural Sciences and Engineering Research Council of Canada (NSERC) is gratefully acknowledged.

References

[1] WorldoMeter. Canada Population (2020). WorldoMeter n.d. https://www.worldometers.info/world-population/canada-population/ (accessed December 25, 2020).
[2] Energy Facts | Natural Resources Canada n.d. https://www.nrcan.gc.ca/science-data/data-analysis/energy-data-analysis/energy-facts/20061 (accessed November 29, 2019).
[3] Hogerwaard J, Dincer I. Comparative efficiency and environmental impact assessments of a hydrogen assisted hybrid locomotive. Int J Hydrogen Energy 2016;41:6894–904. https://doi.org/10.1016/j.ijhydene.2016.01.118.
[4] Marin GD, Naterer GF, Gabriel K. Rail transportation by hydrogen vs. electrification - Case study for Ontario Canada, I: Propulsion and storage. Int J Hydrogen Energy 2010;35:6084–96. https://doi.org/10.1016/j.ijhydene.2010.03.098.
[5] Marin GD, Naterer GF, Gabriel K. Rail transportation by hydrogen vs. electrification - Case study for Ontario, Canada, II: Energy supply and distribution. Int J Hydrogen Energy 2010;35:6097–107. doi:10.1016/j.ijhydene.2010.03.095.
[6] Hong Z, Li Q, Han Y, Shang W, Zhu Y, Chen W. An energy management strategy based on dynamic power factor for fuel cell/battery hybrid locomotive. Int J Hydrogen Energy 2018;43:3261–72. https://doi.org/10.1016/j.ijhydene.2017.12.117.
[7] Meegahawatte D, Hillmansen S, Roberts C, Falco M, McGordon A, Jennings P. Analysis of a fuel cell hybrid commuter railway vehicle. J Power Sources 2010;195:7829–37. https://doi.org/10.1016/j.jpowsour.2010.02.025.
[8] Shinde AM, Dikshit AK, Singh RK, Campana PE. Life cycle analysis based comprehensive environmental performance evaluation of Mumbai Suburban Railway. India. J Clean Prod 2018;188:989–1003. https://doi.org/10.1016/j.jclepro.2018.04.022.
[9] Zhang W, Li J, Xu L, Ouyang M, Liu Y, Han Q, et al. Comparison study on life-cycle costs of different trams powered by fuel cell systems and others. Int J Hydrogen Energy 2016;41:16577–91. https://doi.org/10.1016/j.ijhydene.2016.03.032.
[10] Progress Rail: 710 series engines. Prog Rail n.d. http://s7d2.scene7.com/is/content/Caterpillar/CM20170915-60253-59723 (accessed January 8, 2020).
[11] EMD 710 diesel engine manual, specs and bolt torques n.d. https://www.barringtondieselclub.co.za/emd/emd-710.html (accessed January 9, 2020).
[12] Çengel YA, Boles MA. Thermodynamics: A Engineering Approach. Eighth. USA: McGraw-Hill Education; 2015. 10.1109/MILCOM.2005.1605829.
[13] Ferguson CR, Kirkpatrick AT. Internal Combustion Engines: Applied Thermosciences. Third Edit. Sussex, UK: Wiley; 2016.
[14] Li ZL, Devianto H, Kwon HH, Yoon SP, Lim TH, Lee HI. The catalytic performance of Ni/MgSiO3 catalyst for methane steam reforming in operation of direct internal reforming MCFC. J Ind Eng Chem 2010;16:485–9. https://doi.org/10.1016/j.jiec.2010.01.058.
[15] Atkinson A, Marquis AJ. Handbook of. Fuel Cells. 2010. https://doi.org/10.1002/9780470974001.f500032.
[16] Sundmacher K, Kienle A, Pesch HJ, Berndt JF, Huppmann G. Molten Carbonate Fuel Cells: Modeling, Analysis, Simulation, and Control. Verlag, Wienheim, Germany: Wiley; 2007. doi:10.1002/9783527611324.
[17] Ahn J, Park SH, Lee S, Noh Y, Chang D. Molten carbonate fuel cell (MCFC)-based hybrid propulsion systems for a liquefied hydrogen tanker. Int J Hydrogen Energy 2018;43:7525–37. https://doi.org/10.1016/j.ijhydene.2018.03.015.
[18] Koh JH, Kang BS, Lim HC. Analysis of temperature and pressure fields in molten carbonate fuel cell stacks. AIChE J 2001;47:1941–56. https://doi.org/10.1002/aic.690470906.
[19] Seyam S. Energy and Exergy Analysis of Refrigeration Systems. Low-temperature Technol., IntechOpen 2019:13. https://doi.org/10.5772/57353.
[20] Badwal SPS, Giddey S, Kulkarni A, Goel J, Basu S. Direct ethanol fuel cells for transport and stationary applications - A comprehensive review. Appl Energy 2015;145:80–103. https://doi.org/10.1016/j.apenergy.2015.02.002.
[21] Semelsberger TA, Borup RL, Greene HL. Dimethyl ether (DME) as an alternative fuel. J Power Sources 2006;156:497–511. https://doi.org/10.1016/j.jpowsour.2005.05.082.
[22] Matzen M, Demirel Y. Methanol and dimethyl ether from renewable hydrogen and carbon dioxide: Alternative fuels production and life-cycle assessment. J Clean Prod 2016;139:1068–77. https://doi.org/10.1016/j.jclepro.2016.08.163.
[23] Yuan W, Frey HC, Wei T, Rastogi N, VanderGriend S, Miller D, et al. Comparison of real-world vehicle fuel use and tailpipe emissions for gasoline-ethanol fuel blends. Fuel 2019;249:352–64. https://doi.org/10.1016/j.fuel.2019.03.115.
[24] McCarty RD, Hord J, Roder HM. Selected Properties of Hydrogen. 1981.
[25] Verhelst S, Turner JW, Sileghem L, Vancoillie J. Methanol as a fuel for internal combustion engines. Prog Energy Combust Sci 2019;70:43–88. https://doi.org/10.1016/j.pecs.2018.10.001.
[26] Pereira LG, Cavalett O, Bonomi A, Zhang Y, Warner E, Chum HL. Comparison of biofuel life-cycle GHG emissions assessment tools: The case studies of ethanol

produced from sugarcane, corn, and wheat. Renew Sustain Energy Rev 2019;110:1–12. https://doi.org/10.1016/j.rser.2019.04.043.
[27] Li Q, Wu G, Johnston CM, Zelenay P. Direct Dimethyl Ether Fuel Cell with Much Improved Performance. Electrocatalysis 2014;5:310–7. https://doi.org/10.1007/s12678-014-0196-z.
[28] Oil US, Co R. Ultra Low Sulfur Diesel Specifications n.d.;98421:98421.
[29] Aspen Technology Inc. Physical Property Data Reference Manual. Aspen Tech 1999:1–392.
[30] Guide AS. Using Aspen Plus ®. 2011.
[31] Peng DY, Robinson DB. A New Two-Constant Equation of State. Ind Eng Chem Fundam 1976;15:59–64. https://doi.org/10.1021/i160057a011.
[32] Kerrebrock JL. Aircraft Engines and Gas Turbines. Second Edi. Massachusetts, USA: The MIT Press; 2012. 10.1007/978-0-230-35686-3_1.
[33] Arora CP. Refrigeration and Air Conditioning. Third. New Delhi: Tata McGraw-Hill Publishing Company Limited; 2009.